Role of surface oxidation in enhancing heat transfer across graphene–water interface via Thermal Boundary Resistance modulation

International Communications in Heat and Mass Transfer 172 (2026) 110364

Contents lists available at ScienceDirect

International Communications in Heat and Mass Transfer

journal homepage: www.elsevier.com/locate/ichmt

Role of surface oxidation in enhancing heat transfer across graphene–water interface via Thermal Boundary Resistance modulation

Fabiano Tarulli [a,b,1], Francesco Maria Bellussi [a,c,1], Marina Provenzano [a], Paolo De Angelis [a], Alessandro Casto [b], Margherita Vittucci [b], Natalia Del Fatti [b,d], Francesco Banfi [b], Paolo Maioli [b], Matteo Fasano [a,*]

[a] Politecnico di Torino, Department of Energy, Corso Duca degli Abruzzi 24, Torino, 10129, Italy
[b] FemtoNanoOptics group, Université de Lyon, CNRS, Université Claude Bernard Lyon 1, Institut Lumière Matière, F-69622, Villeurbanne, France
[c] Empa, Swiss Federal Laboratories for Materials Science and Technology, Chemical Energy Carriers and Vehicle Systems Laboratory, 8600 Dübendorf, Switzerland
[d] Institut Universitaire de France (IUF), France

ARTICLE INFO

Dataset link: https://github.com/Fabber12/water-graphene_oxide.git

Keywords:
Graphene
Kapitza resistance
Thermal boundary resistance
Heat transfer
Water
Molecular dynamics

ABSTRACT

Functionalization or surface oxidation is a fundamental requirement for carbon-based nanoparticles to prevent self-aggregation and thus be homogeneously dispersed in a fluid. However, the presence of functional or oxidation groups dramatically affects the thermal boundary resistance (TBR) and thus the overall thermal properties of the resulting colloidal suspension. In this work, we systematically investigate through molecular dynamics simulations the effect of oxidation degree on the TBR at the graphene–water interface. We find a linear correlation between the oxidation degree and the thermal boundary conductance (reciprocal of TBR) at low-to-moderate degrees, which can be interpreted through a parallel thermal resistance model, considering the contributions of pristine graphene and hydroxyl (-OH) groups, confirming our previous experimental findings. Results are interpreted in the light of wettability, roughness and phonon density of states, which highlight the higher affinity between water and graphene as the oxidation degree rises. More generally, beyond the specific case study discussed in this work, this systematic approach can be applied to other solid–liquid interfaces to further explore the general correlation between TBR and surface oxidation degree.

1. Introduction

The thermal boundary resistance (TBR), also known as Kapitza resistance (R_K), arises from interfacial phonon scattering [1–3] and serves as a critical parameter in nanoscale thermal transport, significantly influencing the heat transfer performance of colloids [4] and composite materials [5] reinforced with nanoinclusions, such as metal nanoparticles, carbon nanotubes or graphene nanoplatelets. Various numerical and experimental methods have been proposed and adopted to measure TBR [6–9]. Molecular dynamics (MD) simulations provide a powerful tool for investigating heat transfer at the nanoscale [10–12], offering precise control and reliable methods to analyze how the physical and chemical properties of interfaces influence the TBR *in silico*.

In this context, Merabia and Termentzidis [13] studied the impact of nanoscale surface roughness on thermal boundary conductance ($1/R_K$), demonstrating that rougher interfaces increase conductance by enhancing phonon scattering across a more effective interfacial area. They highlighted that specific interfacial shapes, such as sinusoidal patterns, optimize conductance more effectively than planar surfaces, suggesting that interface morphology plays a crucial role in thermal transport. Furthermore, Alexeev et al. [7] identified a correlation between water layering around graphene and TBR, using non-equilibrium molecular dynamics (NEMD). Further progress in the field of graphene-based composites has highlighted the importance of defect engineering, molecular chain regularity, density, and surface functionalization in enhancing phonon coupling and interfacial heat transfer efficiency [14–16].

In terms of chemical characteristics, Chen et al. [17] studied the effect of functionalization with alkane chains, observing an improvement in the thermal boundary conductance at the water-graphene interface. They also reported changes in the phonon density of states due to graphene functionalization, emphasizing the impact of chemical modifications on vibrational properties. Following these insights, Peng et al. [18] demonstrated that controlling the interfacial struc-

* Corresponding author.
E-mail address: matteo.fasano@polito.it (M. Fasano).
[1] These authors contributed equally to the work.

https://doi.org/10.1016/j.icheatmasstransfer.2025.110364

Available online 7 January 2026

ture can significantly reduce TBR. By introducing a superlattice structure between graphene and water, they achieved a 40% reduction in Kapitza resistance, attributed to enhanced phonon scattering within the graphene layer, which indirectly facilitated heat transfer across the solid–liquid interface.

Recent studies have also highlighted the key role of structural defects in modulating TBR. For example, Zhang et al. [19] found that specific types of defects at the graphene–water interface can reduce TBR by up to 30%. Collectively, these results suggest that controlled interfacial modifications, via oxidation or structural adjustments, can significantly improve heat transfer at solid–liquid interfaces, offering new strategies for optimizing thermal transport in nanofluids and nanocomposites.

Improving heat transfer at the graphene–water interface is also of broad technological relevance, spanning applications in micro- and nano-electronics cooling [20], solar-driven interfacial desalination and evaporation [21], as well as nanofluids and microfluidic systems where interfacial thermal resistance strongly limits heat-dissipation efficiency [22]. These contexts further highlight the importance of understanding how surface chemistry and interfacial structure govern energy transfer across graphene–water heterojunctions.

In our previous MD study [23], we explored the effect of surface wettability on water infiltration and TBR at the interface between water and CNTs. We evaluated this effect using a simplified model, in which we varied the Lennard-Jones parameters [24] describing the water–carbon nanoparticles interaction to mimic different CNT hydrophilic/hydrophobic behavior. However, this approach did not account for specific chemical modifications of the surface. Subsequently, in a recent experimental work, we evaluated the TBR of similar carbon-based materials and water using ultrafast optical spectroscopy [6]. This investigation underscored the fundamental role of surface functionalization of carbon-based nanoparticles, which was essential to achieve an optimal dispersion in solution. The functional groups employed were –OH (hydroxyl) groups, which were covalently bonded to the solid surfaces. Due to the nature of the –OH group, surface functionalization or surface oxidation improved heat transfer between the carbon surface and the surrounding fluid, thus modifying the effective TBR [6]. Based on these findings, this study systematically explores, through MD simulations, how the oxidation degree (defined as the ratio of graphene carbon atoms bonded to hydroxyl groups to the total number of carbon atoms) affects TBR. With a particular focus on graphene oxide–water interfaces, this work expands the microscopic understanding of our previous experimental findings [6]. For this purpose, we designed seven graphene models with oxidation degrees ranging from 0% to 80%, encompassing both pristine graphene and graphene oxide (GO), and employed the approach-to-equilibrium molecular dynamics (AEMD) method [23,25], which allowed us to directly compute the TBR by simulating the relaxation of a temperature gradient across the interface. Our results corroborated our experimental observations, showing a linear relationship between the reciprocal value of the interfacial resistance and the degree of oxidation, at least up to a certain threshold. Additionally, we evaluated the contact angle (CA), the work of adhesion, the surface roughness, the water density profile and the phonon density of states (PDOS), observing enhanced wettability and increased overlap between graphene and water spectra with higher oxidation degrees, which further substantiates our predictions regarding TBR.

2. Materials and methods

2.1. Model building and computational details

MD simulations were carried out using LAMMPS software [26]. The initial topology of pristine graphene was created with VMD [27], and the input LAMMPS data and files with Moltemplate [28]. In the case of AEMD and PDOS simulations, the generated graphene sheet measured $\sim 7.2 \times 7.2$ nm^2, whereas for the CA simulations it measured about $\sim 22 \times 22$ nm^2.

The graphene sheets were functionalized by bonding some carbon atoms chosen randomly with hydroxyl groups (see Fig. 1a). We employed 7 models with different oxidation degrees, namely: 0%, 5%, 10%, 20%, 40%, 60%, and 80% to be simulated (see Fig. 1b–e and Supporting Notes S1 and S2 for further details). We utilized an in-house code for this purpose, which is available on GitHub (see Appendix A). The model investigated here was explicitly limited to basal-plane hydroxylation as a simplified representation of GO functionalization. It corresponded to a subset of the Lerf–Klinowski structural framework, in which hydroxyl and epoxy groups are randomly distributed across the basal plane, while carboxyl and carbonyl functionalities are primarily located at sheet edges [29–31].

The graphene sheet was then included in a box filled with three-body water molecules (see Supporting Note S2). Subsequently, the system was equilibrated in the NPT ensemble by applying an anisotropic barostat at 1 atm along the three orthogonal directions (time constant τ_P of 1 ps) and two separate Langevin thermostats set to 298 K for the liquid and solid phases (time constant τ_T of 0.1 ps) [32]. The equilibration was performed until the potential energy of the system asymptotically reached a steady state value, which typically required around 2 ns.

All simulations were performed with a 1 fs timestep and velocity-Verlet integration scheme [33]. We employed a hybrid force field approach to model the system. The Tersoff potential [34] was used for carbon–carbon interactions in the graphene structure, while the COMPASS force field [35,36] was applied to describe both bonded and non-bonded interactions of water molecules and hydroxyl groups. The hybrid potential scheme adopted here was selected to balance structural accuracy and realistic hydrogen bonding at the solid–liquid interface.

Notably, benchmarks for bilayer graphene report large quantitative differences between Tersoff, REBO and AIREBO depending on the chosen observable, and highlight that different potentials reproduce different aspects of the phonon spectrum with varying accuracy [37]. Since our simulations do not model bond breaking and the carbon lattice mainly provides a mechanically stable vibrational support for interfacial heat exchange, a non-reactive C–C potential such as Tersoff is appropriate for our framework, and replacing it with a reactive force field would add substantial computational cost [38]. Moreover, Tersoff potential has been successfully employed in GO–water simulations using comparable hybrid frameworks. In particular, S. Don et al. [39] validated the use of a Tersoff-based description for the GO backbone against *ab initio* molecular dynamics, showing reliable reproduction of interfacial water structuring and orientation for moderate oxidation degrees. The applicability of this potential at high oxidation levels is more uncertain; however, all simulated systems remained structurally stable, and the linear trend in thermal boundary conductance is established within the oxidation range where the force-field combination is expected to be most reliable.

The choice to adopt the COMPASS force field, rather than the potentials employed in our previous MD work [23], was motivated by the need to accurately capture the physico-chemical behavior of surface-functionalized graphene in a condensed-phase environment. In particular, COMPASS is well-suited for systems involving hydrogen bonding, making it especially appropriate for modeling interfacial phenomena between water and oxidized carbon surfaces. Electrostatic interactions were incorporated using partial atomic charges assigned to water, hydroxyl groups, and the graphene carbon atoms bonded to hydroxyl groups, ensuring net zero charge in the simulation box.

C–O and O–H bonded interactions were then described using the COMPASS force field, while C–C interactions were treated with the Tersoff potential (non-reactive); during model construction, hydroxyl groups (–OH) were covalently grafted onto randomly selected basal-plane carbon atoms (see Fig. 1 and Table S2), and the resulting C–O bonds were kept intact throughout the simulation; no chemical

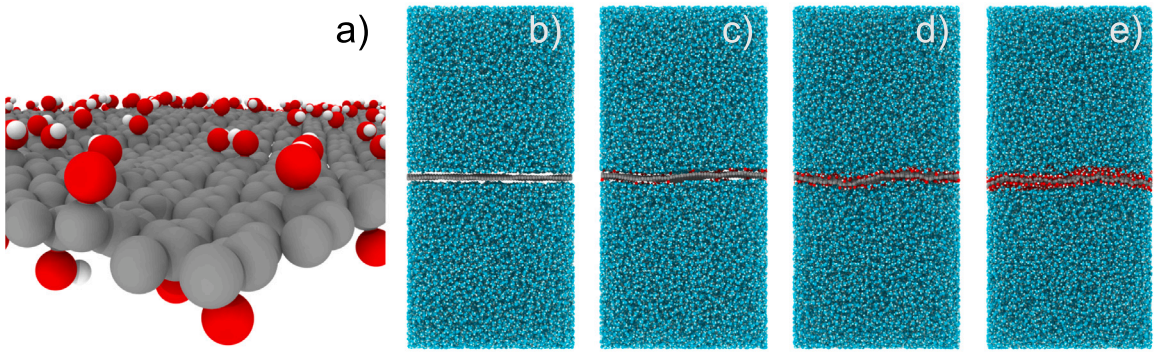

Fig. 1. (a) Pictorial view of a simulated GO sheet. Colors correspond to different atoms: gray = carbon, red = oxygen, and white = hydrogen. Pictorial views of four molecular dynamics systems for different oxidation degrees: (b) 0%, (c) 5%, (d) 40%, and (e) 80%. Systems with 10%, 20% and 60% oxidation are not shown for simplicity. We rendered water molecules in blue and cyan to highlight graphene and hydroxyl groups in gray and red/white, respectively. (For interpretation of the references to color in this figure legend, the reader is referred to the web version of this article.)

reactions were modeled. A cutoff of 1.2 nm was considered to compute the non-bonded interactions, which were described using a 9–6 Lennard-Jones potential with Lorentz–Berthelot mixing rules for cross interactions, and the PPPM method with 10^{-4} accuracy was adopted for the long-range electrostatic interactions [40].

2.2. Calculation of thermal boundary resistance

Thermal boundary resistance was calculated using the AEMD method, following the approach proposed by Jabbari et al. [25], with details on the theoretical framework available in [23]. In this method, the graphene sheet is initially heated to a higher temperature than the surrounding water environment by applying two Langevin thermostats, set at 360 K and 298 K, respectively, with a thermostat coupling constant $\tau_T = 0.1$ ps. Then, the system is left free to relax in the NVE ensemble, while recording the temperature difference between graphene and water and the associated total energy variation of graphene. Then, following Jabbari et al. [25] method, the TBR (indicated as R_K) can be evaluated through:

$$E(t) = E_0 - \frac{S}{R_K}\int_0^t \left[T_p(t') - T_a(t')\right] dt', \tag{1}$$

where $E(t)$ is the energy of graphene at time t, E_0 the constant background energy, $T_p(t)$ the temperature of graphene, $T_a(t)$ the temperature of the surrounding water, and S the graphene–water interface area. As T_a, T_p, and E are computed at each simulation timestep, and E_0 and S are predefined for the given setup, R_K can be determined by fitting the MD trajectories to extract the best-fit value of $-\frac{S}{R_K}$. A detailed explanation of the fitting and integration protocol with related pseudocode is available in Supporting Note S3. Ten independent repetitions were performed for each simulated configuration, and the average and standard error of R_K were calculated accordingly.

The interfacial thermal resistance values reported in this work should be interpreted at a reference temperature equal to the initial water temperature, i.e. $T_{\text{ref}} = 298$ K, consistently with the approach of Alosious et al. [9], given the much larger number of water molecules compared to GO atoms. Alongside this reference-temperature consideration, the robustness of the extracted R_K with respect to the imposed initial overheating of graphene was assessed by varying the initial graphene temperature in additional AEMD simulations. Only negligible variations were observed in the resulting R_K values, confirming the stability and reliability of the extraction procedure. Further details are reported in the Supporting Note S4.

$T_a(t)$ was computed considering only water molecules in the proximity of the graphene surface. This interfacial region was determined by analyzing the water density profile during the MD simulations. After the equilibration process (see Section 2.1), the water density profile was evaluated along trajectories of 1.5 ns each under NPT ensemble (Langevin thermostat on the whole system, 298 K). In detail, we divided the liquid phase into bins of 0.1 Å thickness, where the upper and lower limits of each bin were defined by the *molecular surfaces* computed according to the method of Xu et al. [41]. These surfaces provided a smooth and physically meaningful representation of the instantaneous graphene/GO–water interface. Therefore, because the graphene surface exhibits ripples and evolves over time, the binning regions used to compute the density profile were dynamically updated at every simulation frame so that their boundaries remained parallel to the instantaneous surface shape. By averaging the number of water molecules in a single bin across all 1500 sampled trajectory snapshots, we effectively computed the mean density profiles of water. For all systems, the boundary of the liquid region near the graphene surface used to estimate $T_a(t)$ was defined as the position of the first minimum following the second peak in the water density profile, both below and above the graphene sheet. This minimum consistently occurred at a normal distance of ±9 Å from the surface across all seven models (see Supporting Note S5). For low surface oxidation, the computed Kapitza resistance was largely insensitive to the chosen thickness of the interfacial water region, with R_K values showing overlapping uncertainties. Above 40% hydroxyl coverage, a mild thickness dependence appeared, reflecting the stronger water structuring and slower relaxation dynamics induced by dense –OH groups (see Supporting Note S6). Since TBR is governed predominantly by the first nanometer of interfacial water [39], a slab thickness of 9 Å was therefore adopted consistently for all systems.

2.3. Calculation of contact angle

The contact angle (CA) of water on the graphene substrates was computed with numerical experiments following the sessile droplet (12,696 water molecules) method, as discussed in our previous work [42]. Since this method links contact angle measurements to surface hydrophilicity, it provides a direct way to evaluate wettability. Graphene sheets were previously relaxed by applying an NPT ensemble at 298 K and 0 atm in their planar directions to accommodate for possible deformations induced by different degrees of surface oxidation (coupling constants: $\tau_T = 0.1$ ps for the thermostat, $\tau_P = 1$ ps for the barostat).

Alongside the water-droplet simulations, we also used the free energy perturbation (FEP) method to compute the water–surface work of adhesion W_{sl} on graphene/GO, allowing us to independently verify the predicted contact angle θ. The Young–Dupré formula was then employed to estimate the static CA [43]:

$$W_{sl} = \gamma_{LV}(1 + \cos(\theta)), \tag{2}$$

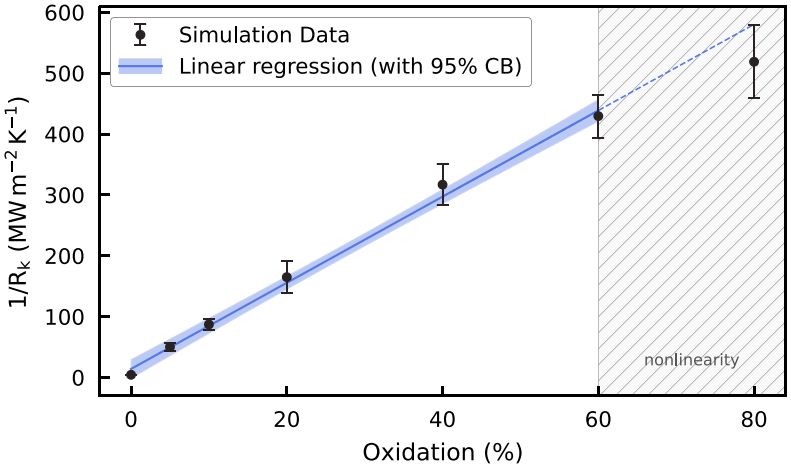

Fig. 2. Thermal boundary conductance ($1/R_K$) at graphene–water interface as a function of graphene oxidation. The black points represent the average simulation results, with vertical uncertainty bars showing the standard error calculated from 10 replicas of each system's simulation. The solid blue line shows the weighted linear regression fitted over moderate oxidation levels (up to 60%), using the relative standard errors as weights. The dashed blue line represents the extrapolation of this linear fit beyond the fitted region. The blue shaded area represents the 95% confidence band (CB) of the regression line. An R-squared equal to 0.995 demonstrates an excellent linear fit, reflecting a high alignment between the regression model and the data. See Supporting Note S8 for tabulated results.

where γ_{LV} is the surface tension of COMPASS model of water, namely 48.1 mJ/m^2 calculated applying the Irving–Kirkwood relation [44].

The updated MATLAB code used to process the MD trajectories for the CA analysis, as well as the implementation of the FEP method, is available in the GitHub repository (see Appendix A).

2.4. Calculation of phonon density of states

The phonon density of states (PDOS) of water and graphene/GO sheets was defined as the Fourier transform of the velocity autocorrelation function (VACF) [17,45]:

$$PDOS = \int_0^{\tau} \langle v(0) \cdot v(t) \rangle \, e^{(-i\omega t)} dt, \tag{3}$$

where $v(0)$ and $v(t)$ are the velocities of the atoms at the initial timestep and at time t, respectively. The velocities were acquired along 400 NVE simulation trajectories lasting 2.5 ps each, with an integration timestep of 1 fs [46]. The decay of the velocity autocorrelation function was monitored to ensure that the sampling time fully captured its relaxation. To obtain the PDOS, the integral in Eq. 3 was computed numerically using a discrete cosine transform (DCT), which preserves the even symmetry of the autocorrelation function and avoids phase artifacts and spectral leakage. The resulting phonon spectra of both water and graphene were then ensemble-averaged over three independent replicas for each oxidation level.

To assess interfacial vibrational matching, we computed the phonon overlap rate S, following Yang et al. [15]:

$$S = \int \omega f(\omega) d\omega, \tag{4}$$

where ω is the vibrational frequency, and $f(\omega)$ represents the cross-over overlap area of the phonons with frequency ω. The influence of the interfacial-water thickness on S was examined by considering slabs of 5, 7, 9, 12, and 15 Å, as well as the bulk region, with no dependence observed. Further details are available in Supporting Note S7.

3. Results and discussion

Having established the simulation methodology, we now examine the computed thermal boundary resistance values. Numerical results indicate that surface oxidation significantly impacts the interfacial heat transfer between graphene and water, decreasing the thermal boundary resistance from (227 ± 19) m^{2}K/GW for pristine graphene to (1.9 ± 0.2) m^{2}K/GW for GO with 80% oxidation. In a previous work, Alexeev et al. reported interfacial thermal boundary resistance values ranging from 10 to 54 m^{2}K/GW, depending on graphene wettability, number of graphene layers, and system pressure, using the Tersoff potential for graphene and the SPC water model [7]. Alosius et al. found TBR values of 12–13 m^{2}K/GW for pristine graphene in both non-equilibrium and equilibrium MD simulations, employing the Tersoff force field and the SPC-E water model [9]. The discrepancy between our results and those of previous molecular studies primarily stems from differences in the underlying molecular models. Notably, both cited works considered only multilayer graphene and did not include single-layer configurations. They also reported a decrease in TBR with increasing graphene layer count, attributed to enhanced overlap of the vibrational density of states at the solid–solid interface. Additionally, differences in the employed water models further contribute to the variation in predicted interfacial thermal transport.

In Fig. 2, we present the Kapitza conductance values, calculated as ($1/R_K$), as a function of the oxidation degree, revealing a linear relationship between the conductance and the oxidation degree up to a certain threshold (60%). This behavior validates the model we developed to interpret the experimental measurements in our previous study at comparable oxidation degrees [6]. Indeed, to analyze the experimental R_K results obtained with oxidized graphene samples immersed in water, we assumed a parallel of thermal resistances between –OH groups and water, and pristine graphene and water. This assumption led us to identify a linear relation between the oxidation degree and the Kapitza conductance [6], namely:

$$\frac{1}{R_K(\alpha)} = \frac{1-\alpha}{R_{K_{0\%}}} + \frac{\alpha}{R_{K_{100\%}}}. \tag{5}$$

In this equation, α (defined as *OH coverage ratio* in [6]) represents the oxidation degree, $R_{K_{0\%}}$ is the Kapitza resistance at the interface between pristine graphene and water, and $R_{K_{100\%}}$ is the Kapitza resistance at the interface between fully oxidized graphene and water. We highlight that, in the previous experimental work [6], a linear trend was hypothesized and then extrapolated to estimate $R_{K_{100\%}}$ and $R_{K_{0\%}}$ based on the two TBRs calculated experimentally with oxidation degrees of $\alpha_1 = 17 \pm 1\%$ and $\alpha_2 = 44 \pm 2\%$. Indeed, the simplified parallel thermal-resistance model assumes an isothermal graphene surface, independent heat-flux channels across pristine and functionalized regions, and a uniform temperature distribution within the interfacial liquid layer.

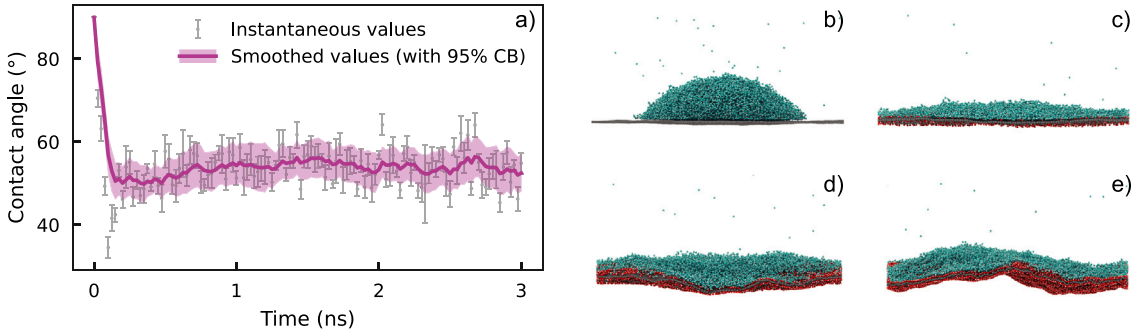

Fig. 3. (a) Variation of the contact angle (CA) on pristine graphene during the stabilization and acquisition trajectory. Instantaneous values with error bars are plotted alongside a smoothed average and its 95% confidence band (CB). The equilibrium value of CA was evaluated over the last 1.5 ns. (b) Pictorial view of a water droplet on pristine graphene corresponding to a CA of ~54°. Pictorial views of full-wetting behavior on GO sheets with (c) 5%, (d) 40% and (e) 80% oxidation degree, respectively. From our simulations, even at low oxidation degrees (*i.e.*, 5%), we observed a significant enhancement in the wettability of GO sheets.

In this context, the MD linear relation describes the behavior of the simulated system but does not serve as a quantitative measure of experimental oxidation levels. For completeness, we report the linear fit $G \equiv 1/R_K(\alpha) = m_{\mathrm{MD}}\alpha + b_{\mathrm{MD}}$, with parameter uncertainties, as well as the inverted relation $\alpha = (G - b_{\mathrm{MD}})/m_{\mathrm{MD}}$ for estimating the hydroxyl coverage within the MD framework (see Supporting Note S9).

Unlike experimental approaches, this study leverages the scalability of MD simulations to systematically investigate multiple oxidation degrees without the constraints of physical sample production. This approach enables us to examine a wider range of oxidation scenarios, verifying the linear relationship between thermal boundary conductance and oxidation degree (see Fig. 2). Notably, while the experimental study extrapolates Kapitza values using Eq. (5), the MD approach enabled a broader exploration of the oxidation spectrum, enhancing the reliability of this linear correlation. Despite differences between the two extraction methods, the linear correlation observed in the MD results offers microscopic evidence supporting the underlying assumption of the model described by Eq. (5), thus providing a solid foundation for extending its applicability to oxidation levels different from those achievable in experiments.

The linear model based on MD results provides a useful and effective description of the data up to an oxidation degree of 60%; beyond this range, we observe deviation from linearity indicating a saturation of the beneficial effects due to the surface roughness. Indeed, the surface roughness increases with the oxidation degree up to 60%, where we observe a plateau (see Supporting Note S10). A qualitatively similar linear-to-saturation transition has been reported by Cui et al. [47], who likewise observe that interfacial conductance increases nearly linearly at low-to-moderate functionalization degrees and then progressively levels off as the surface becomes densely covered.

The linear increase in thermal boundary conductance observed with the degree of oxidation is further examined in relation to the wetting and vibrational properties of the simulated graphene samples. By comparing the results for the CA simulations, we observe that, consistently with our previous numerical work [23] and other studies in the literature [7,25], greater surface wettability leads to higher thermal boundary conductance. The evolution of a water droplet onto the pristine graphene surface is shown in Fig. 3a, where equilibrium conditions are reached after some 1000 ps of simulation. The CA is measured during the last 1.5 ns of the trajectory, where the CA oscillates around a stable mean value of 54°± 5°. Moreover, an independent estimate obtained through FEP yields a contact angle of approximately 57°, providing additional confirmation of the computed value. The water affinity of pristine graphene is confirmed by an experimental study in which the CA of water on graphene was obtained using the captive bubble method, observing a value of 42°± 3° [48]. It is important to mention that calculating the exact value of the contact angle of water on the graphene surface is beyond the scope of this work, since it has been demonstrated that its value is strongly dependent on the experimental conditions as well as model adopted [49].

CA simulations of GO show that even a 5% oxidation degree markedly enhances the wettability of the graphene surface, resulting in complete spreading of water and strong adsorption onto the oxidized regions (Fig. 3c–e). This behavior stems from (i) strengthened water–surface interactions due to charge redistribution over the functionalized graphene, and (ii) surface roughness introduced by the oxygenated groups, which disrupts the atomically smooth structure of pristine graphene. Consequently, in agreement with previous findings [7], the thermal boundary conductance at the graphene–water interface increases with rising surface hydrophilicity. This enhancement is attributed to improved interactions between the solid surface and the interfacial fluid (see Supporting Notes S11 and S12 for a detailed analysis with pristine graphene and GO, respectively), facilitating more efficient heat transfer.

Finally, we calculated and compared the PDOS between water and graphene, presenting in Fig. 4 its variation across different graphene oxidation levels (0% to 80%) and the consequent increment in the overlap between the water and graphene spectra. As previously noted [7,17,50], the higher the overlap, the easier the phonon transfer from one phase to another, therefore enhancing the thermal conductance at the interface.

Overall, the observed decrease in TBR with increasing graphene oxidation arises from such a complex interplay between enhanced wettability, increased PDOS overlap, and surface roughness. These contributions display a linear trend at low-to-moderate oxidation degree. At high oxidation, however, both vibrational and geometric effects begin to saturate: spectral broadening and mode competition limit further gains in overlap (Supporting Note S7), while roughness first stabilizes and then slightly decreases (Supporting Note S10), reducing the effective contribution of additional functional groups. This specific behavior is consistent with the findings of Merabia and Termentzidis [13], who observed that roughness-driven enhancements persist only while the true interface area continues to grow; in our systems, however, roughness effects act together with additional interfacial mechanisms associated with solid–liquid heat transfer.

Taken together, these factors indicate that a linear model provides a reasonable description at low-to-moderate oxidation, with modest deviations emerging as the surface becomes densely functionalized. In this regime, numerical results show that the behavior can be effectively captured by treating the interface as a parallel network of lumped thermal resistances (Eq. (5)), offering a simple yet powerful framework for describing the impact of surface oxidation on interfacial heat transfer.

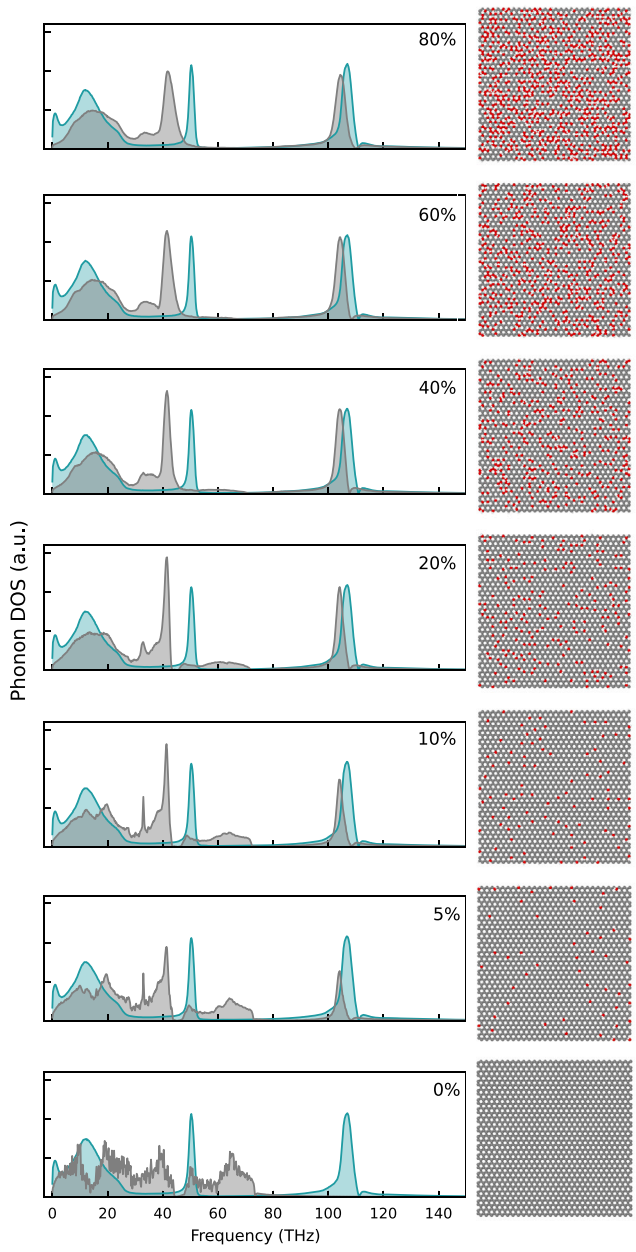

Fig. 4. Phonon density of states (DOS) at graphene/GO–water interfaces for different oxidation degrees, highlighting differences in vibrational modes between pristine graphene/GO (gray) and water (cyan) across the frequency spectrum. Low-frequency modes are related to the molecular motion of liquid, while sharp peaks identify specific bond vibrations. (For interpretation of the references to color in this figure legend, the reader is referred to the web version of this article.)

4. Conclusions

In this work, we used molecular dynamics simulations to evaluate the effect of graphene oxidation on the heat transfer mechanism at the interface with water. In detail, we evaluated the thermal boundary resistance by applying the approach-to-equilibrium molecular dynamics. We developed seven graphene models with oxidation degrees in the range 0%–80%, considering hydroxyl groups only. MD simulations in this work demonstrate that the TBR varies significantly with surface oxidation, showing that its inverse (thermal boundary conductance) increases linearly as oxidation increases. Importantly, the linear trend persists only up to an oxidation degree of 60%, while the saturation occurring at higher levels is accounted for by surface-roughness effects identified through the MD analysis.

These results confirm recent experimental findings on similar carbon nanomaterials obtained employing ultrafast optical spectroscopy [6]. The findings of this work align with observations from our numerical MD simulations [23], which demonstrated a reduction in thermal boundary resistance with increasing wettability. There we employed a toy model in which we varied the Lennard-Jones interaction parameters to mimic different wettability conditions. Here, instead, we adopted a model that responds to the actual physicochemical characteristics of GO. The wettability of graphene is significantly affected by surface functionalization, reaching full wetting conditions at 5% of oxidation already.

While our findings highlight the role of hydroxyl groups in modulating TBR, the interplay between phonon overlap and molecular layering of interfacial water remains complex and context-dependent, with some mechanisms yet to be fully understood at the GO–water interface. We also acknowledge that the proposed model is not a complete description of GO, as it focuses solely on hydroxyl groups while neglecting other functional groups, such as epoxy species on the basal plane and carboxyl or carbonyl groups at sheet edges. This simplification may influence both the wettability and the vibrational coupling at the interface. In perspective, we consider including other functional groups and defects, to refine our model and improve the matching with experimental data. Further improvement relies on the adoption of intermolecular parameters that can reproduce with higher accuracy the contact angle of water onto graphene, guided by experimental data [49]. Finally, we also consider adopting equilibrium molecular dynamics simulations to compare different numerical methods. The reported results can inform the rational design of stable colloidal suspensions with improved heat transfer performance.

CRediT authorship contribution statement

Fabiano Tarulli: Writing – original draft, Visualization, Software, Methodology, Investigation, Formal analysis, Data curation. **Francesco Maria Bellussi:** Writing – original draft, Visualization, Validation, Software, Methodology, Investigation. **Marina Provenzano:** Writing – review & editing, Validation, Software, Methodology. **Paolo De Angelis:** Writing – review & editing, Visualization, Validation, Methodology, Formal analysis. **Alessandro Casto:** Writing – review & editing, Validation, Methodology. **Margherita Vittucci:** Writing – review & editing, Validation. **Natalia Del Fatti:** Writing – review & editing, Validation, Supervision. **Francesco Banfi:** Writing – review & editing, Validation, Supervision, Methodology, Conceptualization. **Paolo Maioli:** Writing – review & editing, Validation, Supervision, Resources, Project administration, Methodology, Conceptualization. **Matteo Fasano:** Writing – review & editing, Validation, Supervision, Resources, Project administration, Methodology, Funding acquisition, Conceptualization.

Declaration of competing interest

None.

Acknowledgments

This work was partially funded by the European Union Horizon Europe Research and Innovation Programme under grant agreement number 101138397 (acronym “M2DESCO”). Views and opinions expressed are however those of the authors only and do not necessarily reflect those of the European Union or the European Health and Digital Executive Agency (HADEA). Neither the European Union nor the granting authority can be held responsible for them. F.T., F.M.B., M.P., and M.F. gratefully acknowledge CINECA (Iscra B project) and the High-Performance Computing Initiative of Politecnico di Torino (http://hpc.polito.it/) for the availability of computing resources and support. We thank Michele Pellegrino and Mokhtar Ganjali Koli for helpful discussions.

Appendix A. Supporting information

Supplementary material related to this article can be found online at https://doi.org/10.1016/j.icheatmasstransfer.2025.110364. The Supporting Information is available free of charge online. The developed simulation data and protocols are available at the GitHub repository associated with this work (https://github.com/Fabber12/water-graphene_oxide.git).

Data availability

The developed simulation data and protocols are available at the GitHub repository associated with this work https://github.com/Fabber12/water-graphene_oxide.git.

References

[1] E.T. Swartz, R.O. Pohl, Thermal boundary resistance, Rev. Modern Phys. 61 (1989) 605.

[2] R. Dettori, C. Melis, X. Cartoixà, R. Rurali, L. Colombo, Thermal boundary resistance in semiconductors by non-equilibrium thermodynamics, Adv. Phys.: X 1 (2016) 246–261.

[3] C. Caddeo, C. Melis, A. Ronchi, C. Giannetti, G. Ferrini, R. Rurali, L. Colombo, F. Banfi, Thermal boundary resistance from transient nanocalorimetry: A multiscale modeling approach, Phys. Rev. B 95 (2017) 085306.

[4] A. Cardellini, M. Fasano, M.B. Bigdeli, E. Chiavazzo, P. Asinari, Thermal transport phenomena in nanoparticle suspensions, J. Phys.: Condens. Matter. 28 (2016) 483003.

[5] A. Chiminelli, I. Radović, M. Fasano, A. Fantoni, M. Laspalas, A. Kalinić, M. Provenzano, M. Fernandes, Modeling carbon-based nanomaterials (cnms) and derived composites and devices, Sensors 24 (2024) 7665.

[6] A. Casto, M. Vittucci, F. Vialla, A. Crut, F.M. Bellussi, M. Fasano, F. Vallée, N. Del Fatti, F. Banfi, P. Maioli, Experimental optical retrieval of the thermal boundary resistance of carbon nanotubes in water, Carbon 229 (2024) 119445.

[7] D. Alexeev, J. Chen, J.H. Walther, K.P. Giapis, P. Angelikopoulos, P. Koumoutsakos, Kapitza resistance between few-layer graphene and water: Liquid layering effects, Nano Lett. 15 (2015) 5744–5749.

[8] Y. Xian, P. Zhang, S. Zhai, P. Yuan, D. Yang, Experimental characterization methods for thermal contact resistance: A review, Appl. Therm. Eng. 130 (2018) 1530–1548.

[9] S. Alosious, S.K. Kannam, S.P. Sathian, B. Todd, Kapitza resistance at water–graphene interfaces, J. Chem. Phys. 152 (2020) 224703.

[10] T. Lin, J. Li, X. Quan, P. Cheng, A molecular dynamics investigation on effects of nanostructures on thermal conductance across a nanochannel, Int. Commun. Heat Mass Transfer 97 (2018) 118–124.

[11] B. Yang, D. Li, H. Yang, J. Wang, P. Yang, Thermal conductivity enhancement of defective graphene nanoribbons, Int. Commun. Heat Mass Transfer 117 (2020) 104735.

[12] H. Liu, S. Ahmad, J. Chen, J. Zhao, Molecular dynamics study of the nanoscale boiling heat transfer process on nanostructured surfaces, Int. Commun. Heat Mass Transfer 119 (2020) 104963.

[13] S. Merabia, K. Termentzidis, Thermal boundary resistance across rough interfaces probed by molecular dynamics, Phys. Rev. B 89 (2014) 054309.

[14] H. Yang, S. Gao, X. Xu, P. Yang, Enhancing heat energy transfer at graphene/polypropylene interface, Appl. Energy 381 (2025) 125134.

[15] H. Yang, S. Gao, Y. Pan, P. Yang, Manipulating heat transfer at graphene/silicon interface with nitrogen doping, Int. Commun. Heat Mass Transfer 155 (2024) 107521.

[16] H. Yang, Y. Shen, L. Li, Y. Pan, P. Yang, Surface modification to induce efficient heat transfer at graphene/silicon heterointerface, Appl. Therm. Eng. 238 (2024) 121913.

[17] S. Chen, M. Yang, B. Liu, M. Xu, T. Zhang, B. Zhuang, D. Ding, X. Huai, H. Zhang, Enhanced thermal conductance at the graphene–water interface based on functionalized alkane chains, RSC Adv. 9 (2019) 4563–4570.

[18] X. Peng, P. Jiang, Y. Ouyang, S. Lu, W. Ren, J. Chen, Reducing kapitza resistance between graphene/water interface via interfacial superlattice structure, Nanotechnology 33 (2021).

[19] X. Zhang, H. Chen, D. Qiao, M.-M. Yang, Effects of structure defects on thermal transport at the graphene–water interface, Adv. Mater. Interfaces 10 (2023).

[20] J. Chen, J.H. Walther, P. Koumoutsakos, Ultrafast cooling by covalently bonded graphene-carbon nanotube hybrid immersed in water, Nanotechnology 27 (2016) 465705.

[21] L. Zang, L. Sun, S. Zhang, C. Finnerty, A. Kim, J. Ma, B. Mi, Nanofibrous hydrogel-reduced graphene oxide membranes for effective solar-driven interfacial evaporation and desalination, Chem. Eng. J. 422 (2021) 129998.

[22] M. Mehrali, E. Sadeghinezhad, A.R. Akhiani, S. Tahan Latibari, S. Talebian, A. Dolatshahi-Pirouz, H.S.C. Metselaar, M. Mehrali, An ecofriendly graphene-based nanofluid for heat transfer applications, J. Clean. Prod. 137 (2016) 555–566.

[23] A. Casto, F.M. Bellussi, M. Diego, N. Del Fatti, F. Banfi, P. Maioli, M. Fasano, Water filling in carbon nanotubes with different wettability and implications on nanotube/water heat transfer via atomistic simulations, Int. J. Heat Mass Transfer 205 (2023) 123868.

[24] T. Werder, J.H. Walther, R. Jaffe, T. Halicioglu, P. Koumoutsakos, On the water-carbon interaction for use in molecular dynamics simulations of graphite and carbon nanotubes, J. Phys. Chem. B 107 (2003) 1345–1352.

[25] F. Jabbari, A. Rajabpour, S. Saedodin, S. Wongwises, Effect of water/carbon interaction strength on interfacial thermal resistance and the surrounding molecular nanolayer of cnt and graphene flake, J. Mol. Liq. 282 (2019) 197–204.

[26] A.P. Thompson, H.M. Aktulga, R. Berger, D.S. Bolintineanu, W.M. Brown, P.S. Crozier, P.J. in't Veld, A. Kohlmeyer, S.G. Moore, T.D. Nguyen, et al., Lammps-a flexible simulation tool for particle-based materials modeling at the atomic, meso, and continuum scales, Comput. Phys. Comm. 271 (2022) 108171.

[27] W. Humphrey, A. Dalke, K. Schulten, Vmd: Visual molecular dynamics, J. Mol. Graph. 14 (1996) 33–38.

[28] A.I. Jewett, D. Stelter, J. Lambert, S.M. Saladi, O.M. Roscioni, M. Ricci, L. Autin, M. Maritan, S.M. Bashusqeh, T. Keyes, et al., Moltemplate: A tool for coarse-grained modeling of complex biological matter and soft condensed matter physics, J. Mol. Biol. 433 (2021) 166841.

[29] A. Lerf, H. He, M. Forster, J. Klinowski, Structure of graphite oxide revisited, J. Phys. Chem. B 102 (1998) 4477–4482.

[30] J.-A. Yan, M.Y. Chou, Oxidation functional groups on graphene: Structural and electronic properties, Phys. Rev. B 82 (2010) 125403.

[31] D.W. Boukhvalov, M.I. Katsnelson, Modeling of graphite oxide, J. Am. Chem. Soc. 130 (2008) 10697–10701.

[32] S.M. Nejad, R. Srivastava, F.M. Bellussi, H.C. Thielemann, P. Asinari, M. Fasano, Nanoscale thermal properties of carbon nanotubes/epoxy composites by atomistic simulations, Int. J. Therm. Sci. 159 (2021) 106588.

[33] W.C. Swope, H.C. Andersen, P.H. Berens, K.R. Wilson, A computer simulation method for the calculation of equilibrium constants for the formation of physical clusters of molecules: Application to small water clusters, J. Chem. Phys. 76 (1982) 637–649.

[34] J. Tersoff, New empirical approach for the structure and energy of covalent systems, Phys. Rev. B 37 (1988) 6991.

[35] H. Sun, COMPASS: An ab initio force-field optimized for condensed-phase ApplicationsOverview with details on alkane and benzene compounds, J. Phys. Chem. B 102 (1998) 7338–7364.

[36] H. Sun, Z. Jin, C. Yang, R.L.C. Akkermans, S.H. Robertson, N.A. Spenley, S. Miller, S.M. Todd, Compass ii: Extended coverage for polymer and drug-like molecule databases, J. Mol. Model. 22 (2016) 47.

[37] X. Zhang, Z. Chen, H. Chen, L. Xu, Comparative studies of thermal conductivity for bilayer graphene with different potential functions in molecular dynamic simulations, Results Phys. 22 (2021) 103894.

[38] T.P. Senftle, S. Hong, M.M. Islam, S.B. Kylasa, Y. Zheng, Y.K. Shin, C. Junkermeier, R. Engel-Herbert, M.J. Janik, H.M. Aktulga, T. Verstraelen, A. Grama, A.C.T. van Duin, The ReaxFF reactive force-field: Development, applications and future directions, Npj Comput. Mater. 2 (2016) 15011.

[39] V. Subasinghege Don, L. Kim, R. David, J.A. Nauman, R. Kumar, Adsorption studies at the graphene oxide–liquid interface: A molecular dynamics study, J. Phys. Chem. C 127 (2023) 5920–5930.

[40] R.W. Hockney, J.W. Eastwood, Computer Simulation using Particles, crc Press, 2021.

[41] D. Xu, Y. Zhang, Generating triangulated macromolecular surfaces by Euclidean distance transform, PLoS One 4 (2009) 1–11.

[42] F.M. Bellussi, O.M. Roscioni, E. Rossi, A. Cardellini, M. Provenzano, L. Persichetti, V. Kudryavtseva, G. Sukhorukov, P. Asinari, M. Sebastiani, et al., Wettability of soft plga surfaces predicted by experimentally augmented atomistic models, MRS Bull. 48 (2023) 108–117.

[43] N.K. Adam, Use of the term 'young's equation' for contact angles, Nature 180 (1957) 809–810.

[44] C. Vega, E. De Miguel, Surface tension of the most popular models of water by using the test-area simulation method, J. Chem. Phys. 126 (2007) 154707.

[45] F.M. Bellussi, C. Sáenz Ezquerro, M. Laspalas, A. Chiminelli, Effects of graphene oxidation on interaction energy and interfacial thermal conductivity of polymer nanocomposite: A molecular dynamics approach, Nanomaterials 11 (2021) 1709.

[46] J. Chen, G. Zhang, B. Li, Tunable thermal conductivity of $si_{1-x}ge_x$ nanowires, Appl. Phys. Lett. 95 (2009) 073117.

[47] H. Cui, I.R. Panneerselvam, P. Chakraborty, Q. Nian, Y. Liao, Y. Wang, Significantly enhanced interfacial thermal transport between single-layer graphene and water through basal-plane oxidation, Carbon 234 (2025) 119910.
[48] A.V. Prydatko, L.A. Belyaeva, L. Jiang, L.M. Lima, G.F. Schneider, Contact angle measurement of free-standing square-millimeter single-layer graphene, Nat. Commun. 9 (2018) 4185.
[49] S.R. Carlson, O. Schullian, M.R. Becker, R.R. Netz, Modeling water interactions with graphene and graphite via force fields consistent with experimental contact angles, J. Phys. Chem. Lett. 15 (2024) 6325–6333.
[50] S. Alosious, S.K. Kannam, S.P. Sathian, B. Todd, Nanoconfinement effects on the kapitza resistance at water–cnt interfaces, Langmuir 37 (2021) 2355–2361.